Controllable Synthesis of a Monophase Nickel Phosphide/Carbon (Ni_5P_4/C) Composite Electrode via Wet-Chemistry and a Solid-State Reaction for the Anode in Lithium Secondary Batteries

Yi Lu, Jiang-Ping Tu, Qin-Qin Xiong, Jia-Yuan Xiang, Yong-Jin Mai, Jun Zhang, Yan-Qiang Qiao, Xiu-Li Wang,* Chang-Dong Gu, and Scott X. Mao*

A monophase nickel phosphide/carbon (Ni_5P_4/C) composite with a thin carbon shell is controllably synthesized via the two-step strategy of a wet-chemistry reaction and a solid-state reaction. In this fabrication, the further diffusion of phosphorus atoms in the carbon shell during the solid-state reaction can be responsible for a chemical transformation from a binary phase of Ni_5P_4-Ni_2P to monophase Ni_5P_4. Galvanostatic charge-discharge measurements indicate that the Ni_5P_4/C composite exhibits a superior, high rate capability and good cycling stability. About 76.6% of the second capacity (644.1 mA h g^{-1}) can be retained after 50 cycles at a 0.1 C rate. At a high rate of 3 C, the specific capacity of Ni_5P_4/C is still as high as 357.1 mA h g^{-1}. Importantly, the amorphous carbon shell can enhance the conductivity of the composite and suppress the aggregation of the active particles, leading to their structure stability and reversibility during cycling. As is confirmed from X-ray-diffraction analysis, no evident microstructural changes occur upon cycling. These results reveal that highly crystalline Ni_5P_4/C is one of the most promising anode materials for lithium-ion batteries.

1. Introduction

Rechargeable lithium-ion batteries (LIBs) are considered as one of the most-promising energy-storage devices.[1,2] In the last decade, great interest has been devoted to searching for new anode materials for next-generation LIBs that can exhibit a higher capacity than graphite while possessing excellent cyclability at the same time for practical applications.[3] Among these various candidates, new conversion electrode materials offer numerous opportunities to reach impressive capacity gains.[4] These electrodes can react electrochemically toward Li^+ by the following conversion reaction: $M_xX_y + ny\text{Li}^+ + ny\text{e}^- \leftrightarrow y\text{Li}_nX + x\ M^0$.

The mechanism of the Li^+ reactivity in the conversion reaction differs from the classical Li^+ intercalation/deintercalation or Li-alloying process, but involves the formation and decomposition of Li_nX. It has been demonstrated that many systems including oxides, sulfides, nitrides, fluorides, and phosphides are suitable as X.[2,5] One of the promising series of anode materials is transition metal phosphides (M-P, where M = Fe, Co, Ni, Cu, etc.) due to their high gravimetric, low polarization, and volumetric capacity associated with the low electrode volume expansion.[6–8] It has been reported that the M-P system exhibits the lowest polarization due to its metallic character and reacts with Li^+ over the lowest and narrowest potential range.[8,9] Boyanov et al.[4] proposed a P-redox mechanism to affirm the conversion reaction and the formation of Li_3P for the M-P system through the insertion process ($M_xP_y + y\text{Li}^+ + y\text{e}^- \rightarrow \text{Li}_yM_xP_y$) and the conversion process ($\text{Li}_yM_xP_y + 2y\text{Li}^+ + 2y\text{e}^- \rightarrow y\text{Li}_3P + xM^0$). Based on these investigations, however, although the M-P system shows a greater capacity than graphite, the capacity retention is somewhat disappointing due to the limited electrode reaction kinetics, and still falls short to be suitable for practical applications.[4,7,10]

In this context, we recently reported the promising performance of the Ni_2P/C nanocomposite as an anode for LIBs.[11] Electrochemical measurements showed a capacity retention of 74.3%, leading to a stable cycling performance. However, after 50 cycles, the reversible capacities were 435 mA h g^{-1} at 0.1 C and 303 mA h g^{-1} at 0.5 C, which are still a little low for high charge-discharge rates. P-rich systems (NiP_2, NiP_3) have a high

Y. Lu, Prof. J.-P. Tu, Q.-Q. Xiong, Y.-J. Mai, J. Zhang, Y.-Q. Qiao, Dr. X.-L. Wang, Dr. C.-D. Gu
State Key Laboratory of Silicon Materials and Department of Materials Science and Engineering
Zhejiang University
Hangzhou, 310027, P. R. China
E-mail: tujp@zju.edu.cn; wangxl@zju.edu.cn
Dr. J.-Y. Xiang
Narada Power Source Co. Ltd., Hangzhou, 311105, P.R. China
Prof. S. X. Mao
Department of Mechanical Engineering and Materials Science
University of Pittsburgh
Pittsburgh, PA 15261, USA

DOI: 10.1002/adfm.201102660

theoretical capacity. However, besides possessing a poor cyclability due to their carbonless condition, they have to be obtained at high temperatures or under complex conditions such as hydrothermal synthesis for a long time.[9,11] The phase transformation from Ni_2P to the binary phase of Ni_2P-Ni_5P_4 at an elevated temperature was reported in work by Berhault et al.[12] Ni_5P_4 has a theoretical capacity of 770 mA h g^{-1} when it is used as an anode material for LIBs. To our knowledge, there are few reports on the application of Ni_5P_4 as anodes. The main reason is that, as shown in the Ni-P phase diagram,[13] it is difficult to synthesize pure Ni_5P_4 through an organic-phase strategy at low temperature based on the kinetics and dynamics processes. It has been reported that monophase Ni_5P_4 has been fabricated by reducing c-$NiPS_3$[12] through H_2 treatment or a two-step strategy including $NaBH_4$-treated Ni powder as the precursor.[14]

Herein, to synthesize monophase Ni_5P_4, after the wet-chemistry reaction, a solid-state reaction was needed to fulfill this goal. Also, we obtained the core/shell structure of the Ni_5P_4/C composite through a wet-chemistry reaction, and the proper thickness of the carbon shell via a solid-state reaction, which has been extensively utilized to improve their various performances by controlling the morphology and structure of the nanomaterials.[15] Therefore, the main goal of this work was to investigate the electrochemical behavior of the new system in detail, namely the monophase Ni_5P_4/C composite, as an anode material for LIBs, subject to the formation of a ternary Li-M-P phase,[16] which is considered to facilitate the Li^+ uptake conversion process after the Li^+ insertion process. It is widely recognized that the aggregation of nanoparticles would result in a poor cycling performance. To enhance the cyclability of the electrode, hybridizing M-P with carbon is effective. The carbon shell can act as a barrier to suppress the aggregation and pulverization of active particles, and thus increase their structure stability during cycling.[17] Also, it has a high electronic conductivity and can improve the conductance of the active materials.[18] Therefore, to advance the application of Ni_5P_4 electrodes with better electrochemical properties, the synthesis of the Ni_5P_4/C composite is an effective way of improving the electrochemical performance including the reversible capacity and cycling stability.

In this present work, a monophase Ni_5P_4/C composite was controllably synthesized via a wet-chemistry reaction: using nickel acetylacetonate ($Ni(acac)_2$) as a metal precursor, trioctylphosphine (TOP) as a phosphorus source, oleic acid (OA) as surfactant agent, and tri-n-octylamine (TOA) as the solvent, at 450 °C in argon for 2 h; and a solid-state reaction: calcination at 500 °C in air for 2 h. The carbon shell on the surface of the Ni_5P_4 spheres offered a conductive layer, increased the structure stability of active particles during cycling, and thus enhanced the capacity retention.

2. Results and Discussion

2.1. Controlled Synthesis of the Monophase Ni_5P_4/C Composite

The Ni-P system with different structures or constituents has been investigated by Schmetterer's group.[13] Here, focusing on the Ni_5P_4 and Ni_2P systems, entirely simply, a two-step reaction strategy accounts for the controlled growth of the monophase

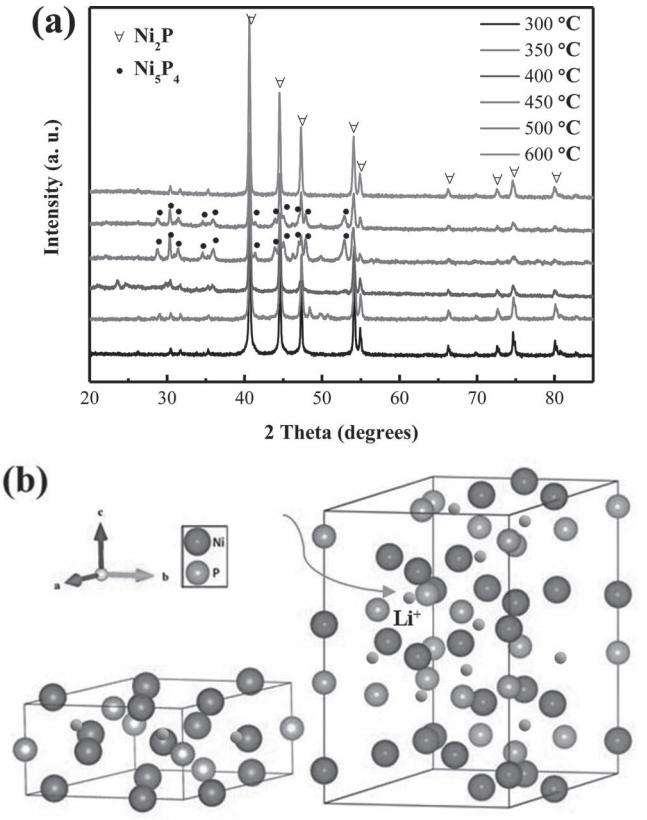

Figure 1. a) XRD patterns of the nickel phosphides after the wet-chemistry reaction for 2 h at different temperatures. b) Schematic illustration of the crystal structure of Ni_2P (left) and Ni_5P_4 (right) with the Li^+ inserted.

Ni_5P_4/C composite from the binary phase of Ni_5P_4 and Ni_2P. **Figure 1**a shows X-ray-diffraction (XRD) patterns of the powders obtained at different wet-chemistry reaction temperatures. As viewed from the dots in this figure, the phase transformation from Ni_2P to the binary phase of Ni_2P-Ni_5P_4 occurred at 450 and 500 °C. All of the peaks match well with Ni_2P (JCPDS 03-0953) and Ni_5P_4 (JCPDS 018-0883). Only Ni_2P existed at other synthetic temperatures. It is interesting that the Ni_5P_4 was observed temporarily and the phase transformation occurred again from the binary phase of Ni_5P_4 and Ni_2P to monophase Ni_2P at 600 °C, which is consistent with the previous literature.[12] For all of the patterns, no other peaks could be observed, indicating that the organic layers possibly introduced in the composites were amorphous. A schematic illustration of the crystal structures of Ni_2P (left) and Ni_5P_4 (right) is shown in Figure 1b. Both the compounds appear to have hexagonal structures. After the phase transformation, the volume of the unit cell became much larger ($a = b = 5.860$ Å, $c = 3.370$ Å for Ni_2P; $a = b = 6.789$ Å, $c = 10.986$ Å for Ni_5P_4; volume = 115.72 $Å^3$ for Ni_2P and 506.35 $Å^3$ for Ni_5P_4) and the density became smaller (7.20 for Ni_2P; 6.32 for Ni_5P_4). It is suggested that the increase in the interspaces between the atoms may facilitate the Li^+ insertion process. Thus, attention has been paid to the samples obtained at the reaction temperatures of 450 °C (S-450) and 500 °C (S-500) due to their special crystal structure, as well as S-400 and S-600, due to their transformation characteristics. From the scanning electron

microscopy (SEM) images of S-450 and S-500 (Figure S1b,c, Supporting Information), one can observe that the nanoparticles were fully covered by thick organic-like shells. Both the powders exhibited non-uniform particle sizes. The nanostructures of S-450 and S-500 were examined further using transmission electron microscopy (TEM), as shown in Figure S1f,g (Supporting Information): nanoparticles with various sizes and thick organic shells of 60 –80 nm for both the composites could be observed. Moreover, the SEM and TEM images of S-400 and S-600 are also shown in Figure S1e,h (Supporting Information). The thickness of the organic shell increased and broken nanoparticles appeared (Figure S1g, Supporting Information) on increasing the reaction temperature. Hollow-structured Ni_2P nanoparticles can be observed in Figure S1e (Supporting Information), which is consistent with previous work.[11,19]

To clarify the applicability of these composites in LIBs, the electrochemical properties with respect to Li^+ insertion/conversion were investigated (Figure S2a, Supporting Information). After 50 cycles, S-450 showed a specific capacity of 465.7 mA h g^{-1} at a current density of 100 mA g^{-1}, which was much higher than that of the others. Therefore, we chose S-450 as the candidate for further investigation.

Although the exact mechanism of the phase transformation from a single crystal phase to a binary phase crystal is not completely understood, but is explained by the slow reduction kinetics of the precursor, this strategy can be helpful for us to control the crystalline phase. As shown in Figure S2b (Supporting Information), the capacity of S-300 decreased quickly to below 100 mA h g^{-1}. Thus, it is imperative that the synthesis of the monophase Ni_5P_4 should be controlled. S-450 was firstly calcined at 400 °C for 2 h in air. The XRD patterns show that the Ni_2P phase still mainly existed (**Figure 2**a). Even when calcined at this temperature for more than 10 h, Ni_2P still existed, except for a little NiO (not shown here). Here, we attempted to calcine S-450 at 500 °C for different times. The weight percentages of the two phases in the composites were estimated using Rietveld refinement of the XRD patterns, which showed that, after calcination at 500 °C for 1 h, the content of the Ni_2P decreased to 7.68% in the Ni_2P-Ni_5P_4 composite, according to the accurate calculation result (see detailed data for the Rietveld refinement in the Supporting Information). After calcination at 500 °C for 2 h, nearly no Ni_2P existed; that is to say, monophase Ni_5P_4 was formed. Typical X-ray photoelectron spectroscopy (XPS) results of the Ni 2p and P 2p region of S-450 after calcination at 500 °C for 2 h (Ni_5P_4/C-2 h) are shown in Figure S3 (Supporting Information). The peaks at 852.2 and 870.8 eV have been assigned to the Ni $2p_{3/2}$ and Ni $2p_{1/2}$ energy levels, respectively. For the P 2p region, the prominent peak at 128.4 eV arose from the P $2p_{3/2}$ and P $2p_{1/2}$ doublet, which has very close binding energies. The difference between Ni 2p and P 2p was 123.8 eV, which is very close to that of Ni_5P_4 reported in the literature.[20] In addition, one can observe obvious satellite peaks in the Ni 2p spectrum, accounting for the oxidation of Ni to Ni^+ or Ni^{2+}. In general, at least 2 h was needed for the complete transformation from Ni_2P-Ni_5P_4 to monophase Ni_5P_4. Therefore, a schematic illustration of the synthetic procedure to obtain the monophase Ni_5P_4/C composite is proposed in **Scheme 1**.

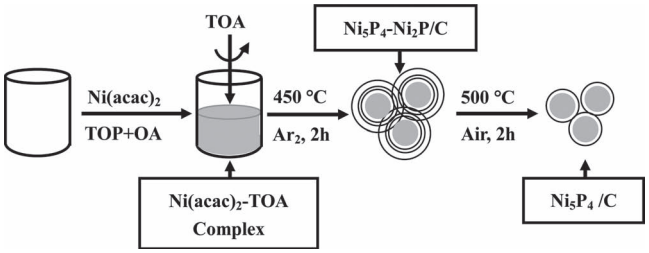

Scheme 1. Schematic illustration of the synthetic procedure of the monophase Ni5P4/C composite.

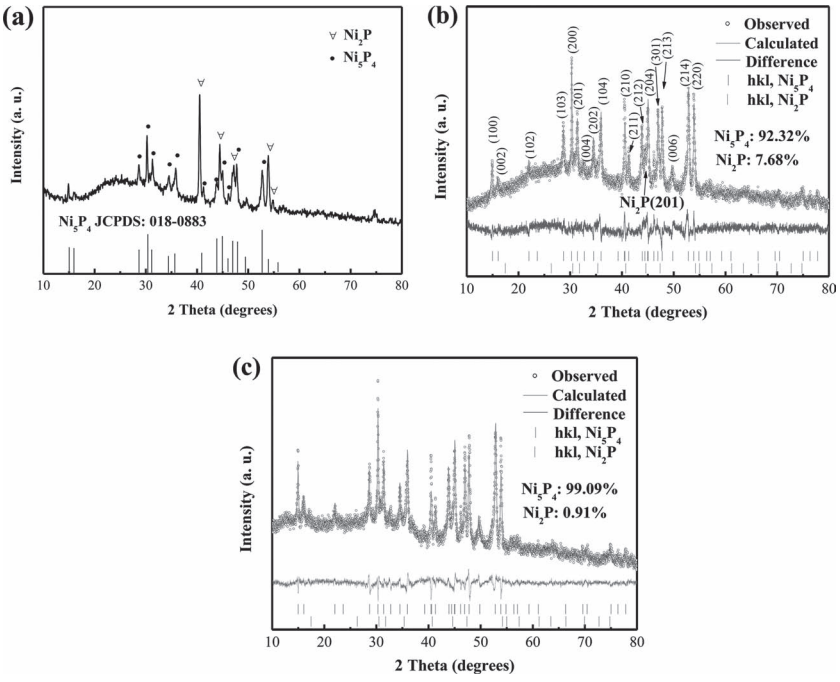

Figure 2. a) XRD pattern of S-450 after calcination in air at 400 °C for 2 h. b,c) Rietveld refined XRD patterns of S-450 after calcination in air for 1 h (b), and 2 h (c).

2.2. Characterization of the Monophase Ni_5P_4/C Composite

It is believed that carbonization would occur in the thick organic layer at a high temperature in air, thus resulting in the formation of a uniform carbon layer. It can be observed using Fourier transform IR (FTIR) spectroscopy that, after the wet-chemistry reaction, weak doublet peaks assigned to C–H stretching and the bending vibration mode still existed, indicating the existence of an organic layer in S-450. However, after the solid-state reaction, no C–H peaks were present, indicating the appearance of an amorphous carbon layer (Figure S4, Supporting Information). **Figure 3**a displays an SEM image of the Ni_5P_4/C composite calcined

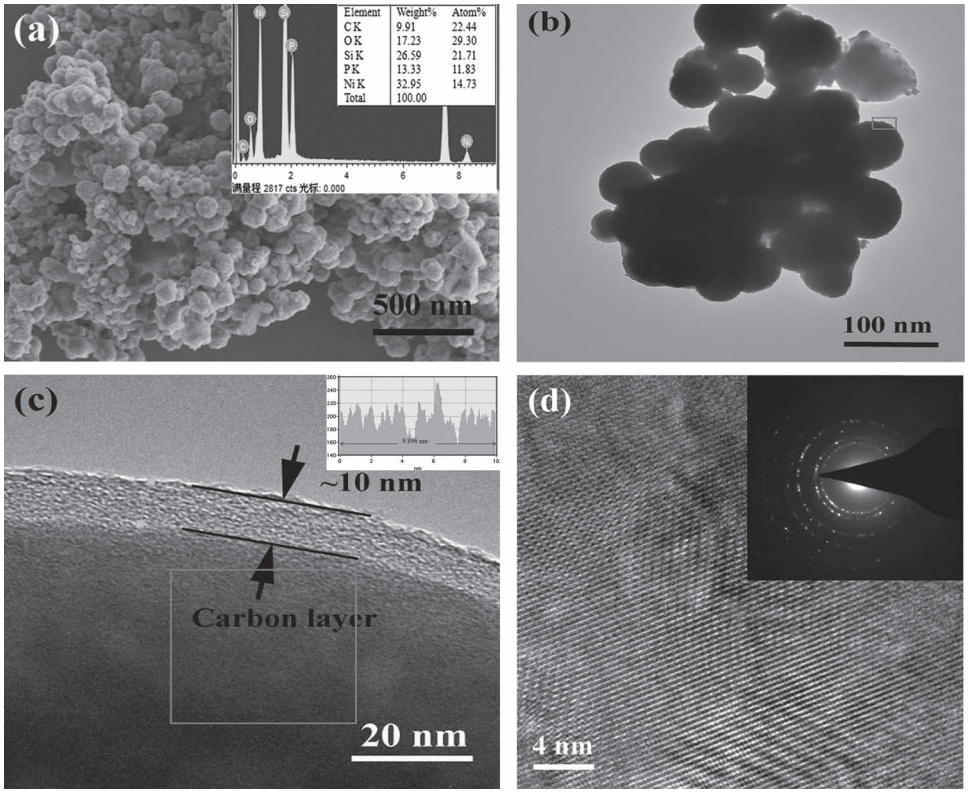

Figure 3. a) SEM image of the Ni_5P_4/C spheres. b) TEM image of the corresponding composite of the Ni_5P_4/C spheres. c) TEM image of an individual Ni_5P_4/C sphere; the inset is the corresponding intensity profile for the line scan across the amorphous carbon shell. d) HR-TEM image and the SAED pattern of the corresponding area in (c).

at 500 °C for 2 h (Ni_5P_4/C-2 h), from which we could observe that, after the solid-state reaction, the thickness of the carbon shell decreased strikingly. The content of carbon in the composite was 9.91 wt%, according to the EDX result. TEM showed that the particles appear to have a sphere-like morphology and a uniform size (Figure 3b). To characterize the structure of the Ni_5P_4/C-2 h composite further, high-resolution TEM (HR-TEM) images are shown in Figure 3c,d. The carbon shell was shown to be amorphous, and the corresponding intensity profile for the line scan across the shell showed that the carbon shell possessed a uniform thickness of about 10 nm (Figure 3c). From Figure 3d, the regularity of the lattice image can be observed. The selected-area electron diffraction (SAED) pattern, as shown in the inset of Figure 3d, revealed the sample to be well-crystallized, and all of the diffraction points could be ascribed to Ni_5P_4 phase. Both the lattice image and the SAED pattern illustrate the polycrystalline nature.

In addition, the morphologies and structures of Ni_5P_4/C-1 h, Ni_5P_4/C-4 h, and Ni_5P_4/C-8 h were also detected, as shown in Figure S5 (Supporting Information). From the SEM image of Ni_5P_4/C-4 h (Figure S5b, Supporting Information), one can also observe uniform grainy nanoparticles, compared with Ni_5P_4/C-1 h and Ni_5P_4/C-8 h (Figure S5a,c, Supporting Information), and the TEM image of Ni_5P_4/C-4 h showed that not only the particles, but also the carbon shell, were partially broken for a longer time of calcination (Figure S5e, Supporting Information). The XRD pattern of Ni_5P_4/C-4 h still exhibited the monophase Ni_5P_4 without NiO. In addition, the particles of Ni_5P_4/C-8 h were broken severely, forming a porous and crumpled structure inside. However, the structure of Ni_5P_4 still maintained a high-crystallinity and only exhibited a hexagonal structure, which also probably accounts for the small content and the amorphous nature of NiO (see the inset of Figure S5f, Supporting Information).

2.3. Growth Mechanism of the Monophase Ni_5P_4/C Composite

To understand the phase-transformation mechanism of the binary phase of the Ni_2P-Ni_5P_4/C to monophase Ni_5P_4/C spheres, thermogravimetric (TG)/DSC curves are presented in **Figure 4**a. There were no obvious reactions below 400 °C according to the corresponding DSC curve, but the reduction in weight of the whole system resulted from the oxidation of the outer carbon layers of the Ni_2P-Ni_5P_4/C nanoparticles in air. It is considered that the further decrease in weight above 400 °C was probably due to the evaporation and decomposition of the inner organic layers.[21] As shown in this figure, the whole weight increased again after 580 °C, indicating that some obvious reactions occurred. The XRD pattern of S-450 calcined at 600 °C for 2 h showed a new phase of NiO (Figure 4b), which is consistent with the increased content of O, as shown in the inset of Figure 3a; that is to say, due to the existence of organic layers, phosphorus in the

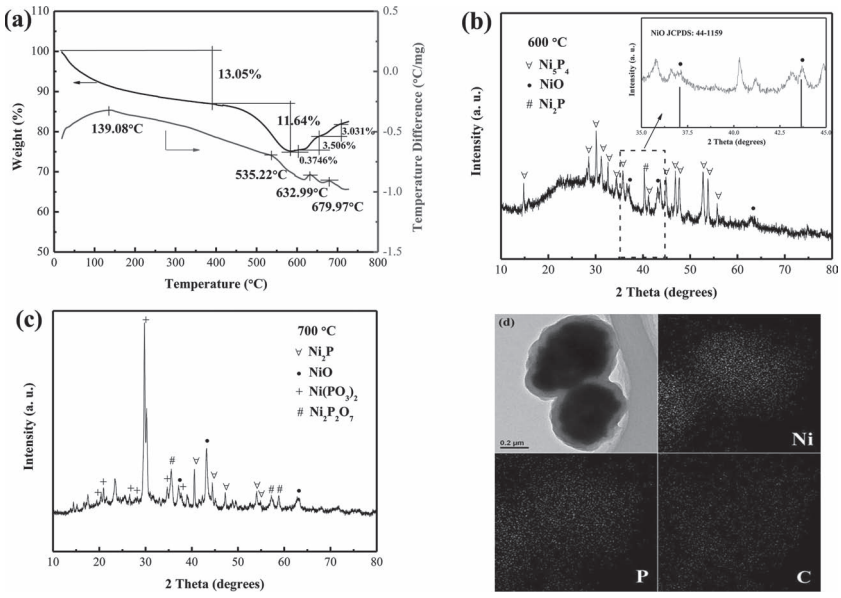

Figure 4. a) TG curve of S-450. b,c) XRD patterns of S-450 calcined at 600 °C for 2 h (b) (the inset in (b) is a magnified pattern of the corresponding dashed square region); and at 700 °C for 2 h (c). d) TEM image of S-450 with the corresponding elemental mapping images for Ni, P, and C.

Ni_5P_4/C composite could not be oxidized. In addition, some phosphates, except for NiO, appeared when the calcination temperature increased to 700 °C (Figure 4c), indicating that the phosphorus in the Ni_5P_4/C composite could be oxidized just at a high temperature (679.97 °C as shown in Figure 4a). Therefore, we consider that there was no nickel or phosphorus obviously being oxidized at 500 °C, which is consistent with the FTIR pectroscopy result in Figure S4 (Supporting Information), that no Ni–O or P–O bonds could be observed. The calcination at 500 °C is the optimized strategy for controlling the phase changes. To investigate the mechanism clearly, elemental mapping images of the Ni, P, and C of S-450 are also illustrated in Figure 4d. After the wet-chemistry reaction, a thick organic layer formed around the particles, also observed from the C signal in accordance with the above FTIR spectroscopy results. As seen from the P signal, the distribution was similar to that of C, and much wider than that of Ni. Therefore, it is believed that, after the wet-chemistry reaction, phosphorus is still scattered in the organic layer in the form of P–C bonds;[22] that is to say, in the TOP layer that has been reported in previous work.[21] This result could also be confirmed by the FTIR-spectroscopy analysis. Then, during the solid-state reaction at 500 °C in air, the P–C bonds break, making the phosphorus diffuse further towards the Ni_2P-Ni_5P_4 particles to form monophase Ni_5P_4 spheres, based on the mechanism of Ostwald ripening. It also can be observed from Figure S4 (Supporting Information) that some peaks assigned to P–C still existed after the wet-chemistry reaction; however, no P–C peaks existed after the solid-state reaction. It is considered that the oxidation of phosphorus was limited by the lower temperature (500 °C compared with 700 °C), the thick organic layers, and the difficulty of cleaving the P–C bonds.[23] Moreover, from the phase transformation of Ni_2P to Ni_5P_4, even to NiP_2, the breaking of the P–C bonds, and further diffusion of phosphorus were limited by the kinetics process, which mainly depends on the temperature. It could be observed that, when the precursors were heated at increased reaction temperatures (300–600 °C) in an argon atmosphere, the solution was gradually dried out, indicating the gradual evaporation and decomposition of these organics and subsequent diffusion of phosphorus.

2.4. Electrochemical Behavior of the Monophase Ni_5P_4/C Composite

The electrochemical behavior of the monophase Ni_5P_4/C composite was evaluated by galvanostatic charge-discharge cycling and cyclic-voltammogram (CV) tests. As shown in **Figure 5**a, a potential window from 0.02 to 3.0 V (versus Li/Li^+) was studied at a constant rate of 0.1 C (≈77 mA h g^{-1}). The initial discharge capacity of the Ni_5P_4/C-2 h composite was as high as

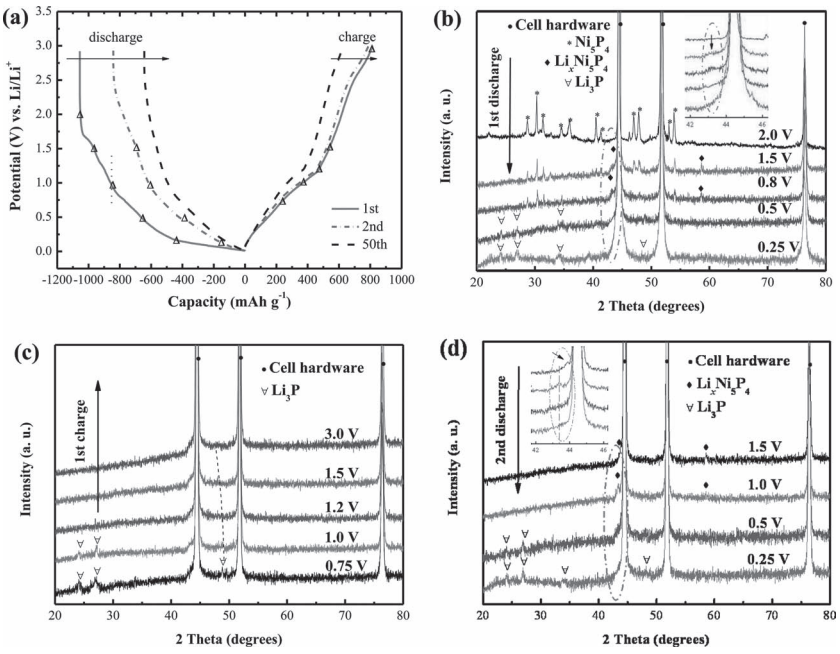

Figure 5. a) The charge/discharge voltage profiles for 1st, 2nd, and 50th cycles for the Ni_5P_4/C-2 h electrode at 0.1 C. b–d) Ex situ XRD patterns of Ni_5P_4/C electrode at different potentials for the first discharge (b), the first charge (c), and the second discharge (d) processes, cycled between 0.02 and 3 V at a rate of C/100.

1055.9 mA h g^{-1}. The extra capacity of the electrode, compared with the theoretical capacity of Ni_5P_4 (≈730 mA h g^{-1} for the Ni_5P_4/C composite containing 9.91 wt% carbon), resulted from the formation of a solid electrolyte interface (SEI) during the first discharging process.[24] The discharge capacity occurred mainly below 0.8 V, and the charge capacity appeared from 0.8 to 1.2 V and 2.5 to 2.8 V. The potential profiles of the Ni_5P_4/C-2 h electrode indicate a plateau in the first discharge and a smoother and sloped shape after the second discharge. The irreversible potential profile at the initial cycles also might be associated with the formation of an SEI layer.[25]

To get deeper insight into the reactions that occurred during the first discharge/charge and the second discharge processes, ex situ XRD patterns of the Ni_5P_4/C electrode at different discharge potentials and at a C/100 rate were investigated, as shown in Figure 5b–d, by labeling some of the significant voltages during the discharge process (Figure 5a). On decreasing the potential, a decrease in the intensity of the main Ni_5P_4 phase was observed. However, as the cell was discharged to 0.8 V, the intensity of the main Ni_5P_4 peaks decreased continuously at the expense of the Bragg peaks at 2θ = 42.5 –43° and ≈58°, which are illustrated by the black diamonds in Figure 5b. It is suggested that these peaks should be assigned to a $Li_xNi_5P_4$ ternary phase. This ternary phase is unknown in the literature and in the Li-Ni-P phase diagram. When the cut-off potential of 0.5 V was selected, we noted the gradual occurrence of the Li_3P phase and the disappearance of this $Li_xNi_5P_4$ ternary phase. Therefore, it is believed that the conversion reaction occurred at the potential of ≈0.8 V, corresponding to the lithiation of 3.5 Li^+. In addition, the peaks of the cell hardware are attributed to the Ni substrate. Thus, the growth of metallic Ni during the discharge process could be observed by the HR-TEM study (which will be discussed below). During the first charge process, the XRD patterns in Figure 5c show a progressive decrease in the Li_3P Bragg peaks. The pattern for the fully charged sample showed no obvious peaks, characteristic of an amorphous electrode. It should be noted that, although some distinct peaks exist in the CV curves during the anodic scanning, no evident structural changes could be observed in these XRD patterns, indicating the homogenous existence of extraction/conversion reactions. These results are similar to those of previous work on the Ni-P system.[8b] Upon subsequent cycles, it showed similar behavior with, namely, the formation of the $Li_xNi_5P_4$ phase and the direct growth of Li_3P (presented here in Figure 5d), and its disappearance during charge (not shown here).

Figure 6a shows CV plots of the Ni_5P_4/C-2 h electrode performed over the potential range of 0 –3.0 V (versus Li/Li^+) at a scanning rate of 0.1 mV s^{-1}. The redox peaks are in accordance with the charge-discharge potential profiles shown in Figure 5a. These redox peaks were indexed to a two-step insertion/conversion process as discussed from the ex situ XRD results. There were mainly four cathodic peaks during the initial discharge process. As we discussed above, among these cathodic peaks, the ones with maxima at 1.7 and 1.25 V correspond to the insertion process. The peaks located at about 0.65 V correspond to the diffusion and conversion processes, namely the full decomposition of Ni_5P_4 into metallic Ni, and the formation of amorphous Li_3P and the SEI layers. During the charging process, the anodic peaks are related to

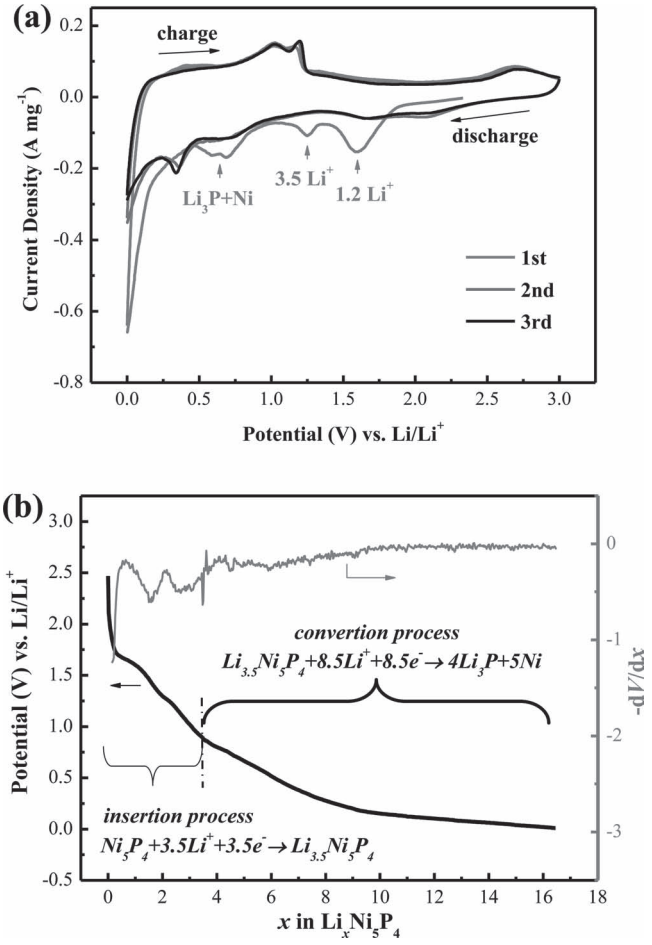

Figure 6. a) CV plots between 0 and 3.0 V (versus Li/Li^+) at a scan rate of 0.1 mV s^{-1}. b) The initial charge-discharge voltage profile showing the x in $Li_xNi_5P_4$ and its associated $-dV/dx$ derivate plot.

the decomposition of the SEI and Li_3P[4,24,26] and to the reversible reaction at about 2.7 V (Figure 6a). After the initial cycle, the former two cathodic peaks, which shifted to near 2.15 and 1.7 V could still be observed, indicating the existence again of the insertion process. The reversible conversion peaks shifted to about 0.65 and 0.3 V, indicating that a diffusion-controlled process became more significant due to the formation of the SEI layer.[27] However, the oxidation peaks had no shift and no attenuation, suggesting good reversibility, possibly due to the carbon shell that was introduced.[11,28]

As shown in Figure 6b, a dashed line has been labeled to present a well-pronounced voltage step near 0.8 V, which was derived from a sudden convex-concave peak near x = 3.5 in $-dV/dx$. This certifies that there were some changes in the reaction process, namely the insertion process (3.0–0.85 V) and the conversion process (0.85–0.02 V). Based on the calculated x in $Li_xNi_5P_4$, the insertion process could be concluded as: $Ni_5P_4 + 1.2Li^+ + 1 - 2e^- \rightarrow Li_{1.2}Ni_5P_4$ and $Li_{1.2}Ni_5P_4 + 2.3e^- \rightarrow Li_{3.5}Ni_5P_4$ The conversion process can be considered as: $Li_{3.5}Ni_5P_4 + 8.5Li^+ + 8.5e^- \rightarrow 4Li_3P + 5Ni$.

Figure 7a gives the first galvanostatic charge-discharge curves of Ni_5P_4/C electrode between 0.02 and 3.0 V (versus Li/Li^+) at

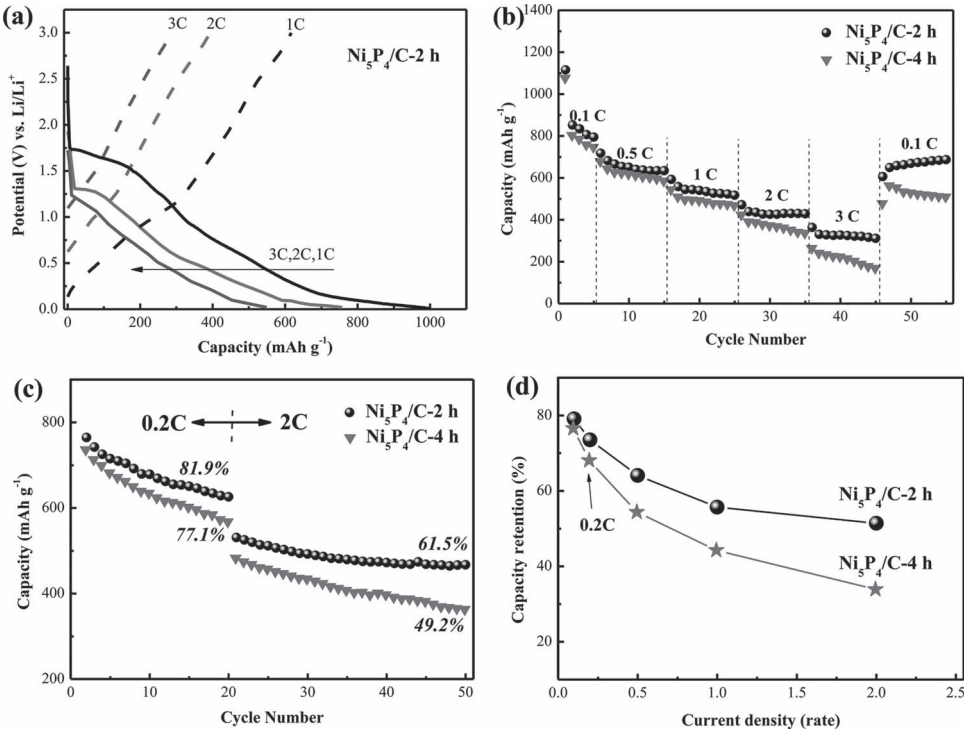

Figure 7. a) Galvanostatic lithium-insertion/extraction curves of the Ni_5P_4/C electrode at rates of 1–3 C. b) Discharge capacity with cycle number under different current rates (0.1–3 C). c) Cycling performance of first 20 cycles at 0.2 C rate followed by another 30 cycles at 2 C rate between 0.02 and 3.0 V. d) Discharge-capacity retention as a function of current density (C).

rates of 1 –3 C. On increasing the rate, separation of the two discharge plateaus gradually became blurred and the plateaus shifted toward low voltages. When the rate was increased to 3 C, the discharge curve exhibited a sloping nature without the obvious plateaus. These phenomena can be explained by the ohmic drop and the increase of cell polarization at high current densities. It is not difficult to understand the results that the capacity loss observed on increasing the rate was due to kinetic limitations and not to some structural changes.[29]

Figure 7b shows the galvanostatic cycling of the cells at charge-discharge rates ranging from 0.1 to 3 C. On increasing the current rate, the discharge capacities of the two composites (Ni_5P_4/C-2 h and Ni_5P_4/C-4 h) decreased gradually, indicating the diffusion-controlled kinetics process for the electrode reaction.[30] It was observed that the Ni_5P_4/C-2 h electrode shows a lower fading rate than Ni_5P_4/C-4 h. At a high rate of 3 C, the specific charge capacity of Ni_5P_4/C-2 h was still as high as 357.1 mA h g^{-1}; however, a rapid decrease of the discharge capacity for Ni_5P_4/C-4 h was observed. When the rate was lowered to 0.5 C, a stable capacity, even an increasing capacity, during cycling was regained for Ni_5P_4/C-2 h, but, for Ni_5P_4/C-4 h, the capacity just showed a high initial value, and then decreased markedly. Compared with Ni_5P_4/C-4 h, the cyclability of the Ni_5P_4/C-2 h electrode was significantly improved, especially at high rate, suggesting that the high-crystallinity and the low density of the unit cell helped the Li^+ transfer; more importantly, the uniform carbon shell in the composite facilitated Li^+ and electron transportation, and also kept the structure stable, to obtain a better capacity retention. The rate capacities of the materials were also investigated at a 0.2 C rate for 20 cycles followed by a 2 C rate for another 30 cycles. The capacity retention of Ni_5P_4/C-2 h was 81.9% at the 0.2 C rate and 61.5% at the 2 C rate (corresponding to the initial value at the 0.2 C rate), respectively, while those of Ni_5P_4/C-4 h were 77.1% at the 0.2 C rate and 49.2% at the 2 C rate (Figure 7c). It is not difficult to understand the result that the capacity loss observed on increasing the current rate was due to kinetic limitations. Near 55% of its capacity for Ni_5P_4/C-2 h could be preserved as the current density increased from 0.1 to 2 C (Figure 7d), much higher than that for Ni_5P_4/C-4 h.

Figure 8 shows the cyclability of the Ni_5P_4/C electrodes at a charge-discharge rate of 0.1 C. The specific reversible capacity of Ni_5P_4/C-2 h after 50 cycles was 644.1 mA h g^{-1}. However, after

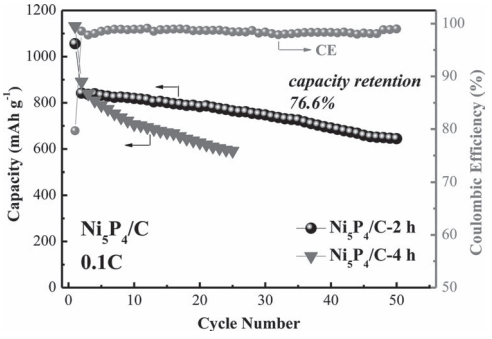

Figure 8. Specific capacity versus cycle number for Ni_5P_4/C electrodes at 0.1 C.

25 cycles, the capacity of Ni_5P_4/C-4 h had already decreased below 600 mA h g^{-1}. In addition, for the Ni_5P_4/C-2 h electrode, 76.6% of its second capacity could still be retained. The good cycling performance is attributed to the carbon shell enhancing the conductivity and keeping the structure stable. This figure also gives the coulombic efficiency of the Ni_5P_4/C electrodes at the 0.1 C rate. The initial coulombic efficiency of the Ni_5P_4/C-2 h was 79.6%. In subsequent cycles, the coulombic efficiency was steady and kept above 99%. All of these results confirm that the Ni_5P_4/C-2 h composite has a better cycling stability than Ni_5P_4/C-4 h due to the perfect carbon shell, which could improve the conductivity of the electrode material, and relieve the strain or accommodate volume expansion/contraction in a timely fashion.[11] Overall, the optimized synthetic strategy for the better electrochemical performance is still calcination at 500 °C in air for 2 h.

2.5. Structural Stability of the Ni_5P_4/C Composite

To obtain a more exact and straightforward investigation of the electrochemical process, HR-TEM and SAED measurements were performed on the cycled electrode. When the Ni_5P_4/C-2 h electrode was fully discharged, the initial particles transformed into an agglomerate of crystallized 5 nm-particles embedded in a crystallized lithiated matrix (**Figure 9**a). These nanoparticles exhibited good dispersion. The so-obtained spots of the SAED shown in Figure 9b could be indexed to a metallic Ni phase, which can also be confirmed in Figure 9a.

The SEM image (Figure S6, Supporting Information) of the fully charged Ni_5P_4/C-2 h electrode was analyzed after 50 cycles. Grainy Ni_5P_4/C composite spheres were still visible, though there was slight aggregation, indicating that the Ni_5P_4/C-2 h composite was stabilized by the carbon shell that was introduced. This accounts for, again, the better reversibility of the Ni_5P_4/C electrode, which is consistent with the cycling performance and CV results.

3. Conclusions

In summary, monophase Ni_5P_4/C composites were synthesized controllably via two reaction steps: a wet-chemistry reaction and a solid-state reaction. On the basis of our investigations, the optimized synthetic strategy is heating at 450 °C for 2 h in argon gas during the wet-chemistry reaction and calcination at 500 °C for 2 h in air during the solid-state reaction. In this approach, highly crystalline Ni_5P_4/C spheres with uniform morphology were obtained. The carbon shell improved the conductivity of Ni_5P_4 spheres, which could facilitate Li^+ and electrons to transfer more easily, and the structural stability, which would contribute significantly to the capacity retention. The Ni_5P_4/C-2 h composite exhibited a high specific capacity and a superior high-rate performance, as well as good cyclic stability, which are attributed to the high-crystallinity nature and the unique core/shell structure. Considering the remarkably improved performance and facile low-temperature strategy, the nanosized Ni_5P_4/C composite could be a promising anode material for LIB applications.

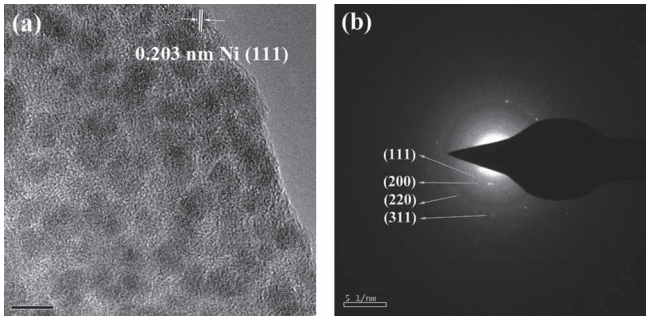

Figure 9. a) HR-TEM image of Ni_5P_4/C-2 h after full discharge to 0.02 V at the 50th cycle. b) The corresponding SAED pattern.

4. Experimental Section

Materials and Synthesis: Hexagonal nickel phosphides (Ni_5P_4, Ni_2P) were prepared by a facile organic-phase strategy similar to that reported by Chen et al.[31] In a typical synthesis, $Ni(acac)_2$ (1 mmol, ≈95%, Sinopharm Chemical Reagent Co.), TOP (7 mmol, ≈97%, J&K Chemical Ltd.), and OA (4 mmol, d = 0.85 g mL^{-1}, Sinopharm Chemical Reagent Co.) were mixed under magnetic stirring. Then, TOA (7 mL, ≈90%, Aladdin Chemistry Co.) was directly added into the mixture under continuous magnetic stirring. Afterwards, the obtained precursor was heated at temperatures ranging from 300 to 600 °C and aged for 2 h under the protection of high-purity argon gas. After cooling to room temperature, the black products were precipitated out by adding a mixture of hexane and ethanol, and separated by centrifugation. The precipitation was washed several times and dried in vacuum. During the solid-state reaction process, the product synthesized at the wet-chemistry reaction temperature of 450 °C was transferred to a muffle furnace and calcined at 500 °C in air for different times. After calcination, the final, black, solid products were filtered, washed with deionized water and absolute ethanol to remove impurities, and dried in an oven at 80 °C overnight.

Characterization of Materials: The crystalline structures of these products were identified by XRD (Rigaku D/max 2550 PC, Cu K_α radiation, λ = 1.5416 Å). The unit-cell lattice parameters were obtained by Rietveld refinement of the powder XRD data using the Maud software.[32] The morphologies and microstructures of these products were characterized using SEM (Hitachi S-4700) and field-emission SEM (FE-SEM) (FEI Sirion-100) equipped with EDX, TEM (JEM 200CX at 160 kV and Tecnai G2 F20 at 200 kV), and XPS (PHI 5700). TG/DSC analysis of the sample was measured on a Netzsch-STA 449C apparatus from 20 to 700 °C at a heating rate of 5 °C min^{-1} in air. The FTIR spectra were collected using a Bruker Vector 33 IR spectrometer by drop-casting the sample solutions onto KBr pellets and pressing the powder to a slice.

Electrochemical Characterization: The working electrodes were prepared by a slurry-coating procedure. The slurry consisted of 80 wt% Ni_5P_4/C composite, 10 wt% acetylene black (AB) and 10 wt% poly(vinylidene fluoride) (PVDF) dissolved in *N*-methyl pyrrolidinone (NMP), and was incorporated on a piece of nickel foam with diameter of 12 mm. After being dried at 90 °C for 24 h in vacuum, the samples were pressed under a pressure of 20 MPa. Test cells (CR 2025) were assembled in an argon-filled glove box with the metallic lithium foil as both the reference and counter electrodes, 1 M $LiPF_6$ in ethylene carbonate (EC)-dimethyl carbonate (DME) (1: 1 in volume) as the electrolyte, and a polypropylene (PP) microporous film (Cellgard 2300) as the separator. The galvanostatic charge-discharge tests were conducted on a LAND battery program-control test system (CT-2001A, Jinnuo electronic Co.) at rates of 0.1–3 C (1 C = 770 mA g^{-1}) in the voltage range of 0.02–3.0 V at room temperature (25 ± 1 °C). CV tests were performed on a CHI660C

electrochemistry workstation (Chenhua instrument Co.) at a scan rate of 0.1 mV s^{-1} between 0 and 3.0 V (versus Li/Li^+).

Supporting Information

Supporting Information is available from the Wiley Online Library or from the author.

Acknowledgements

This work was supported by the Fundamental Research Funds for the Central Universities (2011QNA4006) and the Key Science and Technology Innovation Team of Zhejiang Province (2010R50013). The authors also thank the help of Dr. Yuewu Zeng, Wei Huang, and Xinting Cong for operating the TEM, and Lei Yi for molecular dynamics simulations.

Received: November 4, 2011
Revised: March 30, 2012
Published online: May 24, 2012

[1] a) A. S. Arico, P. Bruce, B. Scrosati, J. M. Tarascon, W. Van Schalkwijk, *Nat. Mater.* **2005**, *4*, 366; b) J. Maier, *Nat. Mater.* **2005**, *4*, 805; c) J. M. Tarascon, M. Armand, *Nature* **2001**, *414*, 359; d) P. Balaya, H. Li, L. Kienle, J. Maier, *Adv. Funct. Mater.* **2003**, *13*, 621; e) W. M. Zhang, X. L. Wu, J. S. Hu, Y. G. Guo, L. J. Wan, *Adv. Funct. Mater.* **2008**, *18*, 3941.

[2] S. L. P. Poizot, S. Grugeon, L. Dupont, J-M. Tarascon, *Nature* **2000**, *407*, 496.

[3] a) M. H. Liang, L. J. Zhi, *J. Mater. Chem.* **2009**, *19*, 5871; b) H. M. Liu, Y. G. Wang, K. X. Wang, E. Hosono, H. S. Zhou, *J. Mater. Chem.* **2009**, *19*, 2835; c) Q. S. Gao, L. C. Yang, X. C. Lu, J. J. Mao, Y. H. Zhang, Y. P. Wu, Y. Tang, *J. Mater. Chem.* **2010**, *20*, 2807; d) F. Gillot, M. P. Bichat, F. Favier, M. Morcrette, M. L. Doublet, L. Monconduit, *Electrochim. Acta* **2004**, *49*, 2325; e) R. Z. Hu, H. Liu, M. Q. Zeng, H. Wang, M. Zhu, *J. Mater. Chem.* **2011**, *21*, 4629; f) B. J. Li, H. Q. Cao, J. Shao, M. Z. Qu, J. H. Warner, *J. Mater. Chem.* **2011**, *21*, 5069.

[4] S. Boyanov, J. Bernardi, E. Bekaert, M. Menetrier, M. L. Doublet, L. Monconduit, *Chem. Mater.* **2009**, *21*, 298.

[5] a) P. Poizot, S. Laruelle, S. Grugeon, J. M. Tarascon, *J. Electrochem. Soc.* **2002**, *149*, A1212; b) L. F. Nazar, D. C. S. Souza, V. Pralong, A. J. Jacobson, *Science* **2002**, *296*, 2012; c) Y. F. Zhukovskii, E. A. Kotomin, P. Balaya, J. Maier, *Solid State Sci.* **2008**, *10*, 491; d) J. Cabana, L. Monconduit, D. Larcher, M. R. Palacin, *Adv. Mater.* **2010**, *22*, E170.

[6] a) V. Pralong, D. C. S. Souza, K. T. Leung, L. F. Nazar, *Electrochem. Commun.* **2002**, *4*, 516; b) K. Wang, J. Yang, J. Y. Xie, B. F. Wang, Z. S. Wen, *Electrochem. Commun.* **2003**, *5*, 480; c) M. G. Kim, J. Cho, *Adv. Funct. Mater.* **2009**, *19*, 1497.

[7] M. Cruz, J. Morales, L. Sanchez, J. Santos-Pena, F. Martin, *J. Power Sources* **2007**, *171*, 870.

[8] a) S. Boyanov, J. Bernardi, F. Gillot, L. Dupont, M. Womes, J. M. Tarascon, L. Monconduit, M. L. Doublet, *Chem. Mater.* **2006**, *18*, 3531; b) F. Gillot, S. Boyanov, L. Dupont, M. L. Doublet, A. Morcrette, L. Monconduit, J. M. Tarascon, *Chem. Mater.* **2005**, *17*, 6327; c) J. Y. Xiang, X. L. Wang, J. Zhong, D. Zhang, J. P. Tu, *J. Power Sources* **2011**, *196*, 379; d) Y. Lu, J. P. Tu, Q. Q.n Xiong, Y. Q. Qiao, X. L. Wang, C. D. Gu, S. X. Mao, *RSC Adv.* **2012**, *2*, 3430.

[9] a) H. Pfeiffer, F. Tancret, M. P. Bichat, L. Monconduit, F. Favier, T. Brousse, *Electrochem. Commun.* **2004**, *6*, 263; b) R. Alcantara, J. L. Tirado, J. C. Jumas, L. Monconduit, J. Olivier-Fourcade, *J. Power Sources* **2002**, *109*, 308; c) J. Y. Xiang, J. P. Tu, X. L. Wang, X. H. Huang, Y. F. Yuan, X. H. Xia, Z. Y. Zeng, *J. Power Sources* **2008**, *185*, 519; d) S. Boyanov, F. Gillot, L. Monconduit, *Ionics* **2008**, *14*, 125.

[10] a) Z. S. Zhang, J. Yang, Y. Nuli, B. F. Wang, J. Q. Xu, *Solid State Ionics* **2005**, *176*, 693; b) H. Pfeiffer, F. Tancret, T. Brousse, *Electrochim. Acta* **2005**, *50*, 4763; c) M. P. Bichat, T. Politova, H. Pfeiffer, F. Tancret, L. Monconduit, J. L. Pascal, T. Brousse, F. Favier, *J. Power Sources* **2004**, *136*, 80.

[11] a) Y. Lu, J. P. Tu, C. D. Gu, X. L. Wang, S. X. Mao, *J. Mater. Chem.* **2011**, *21*, 17988; b) Y. Lu, J. P. Tu, J. Y. Xiang, X. L. Wang, J. Zhang, Y. J. Mai, S. X. Mao, *J. Phys. Chem. C* **2011**, *115*, 23760.

[12] H. Loboue, C. Guillot-Deudon, A. F. Popa, A. Lafond, B. Rebours, C. Pichon, T. Cseri, G. Berhault, C. Geantet, *Catal. Today* **2008**, *130*, 63.

[13] C. Schmetterer, J. Vizdal, H. Ipser, *Intermetallics* **2009**, *17*, 826.

[14] a) K. Senevirathne, A. W. Burns, M. E. Bussell, S. L. Brock, *Adv. Funct. Mater.* **2007**, *17*, 3933; b) R. E. Schaak, A. E. Henkes, *Chem. Mater.* **2007**, *19*, 4234.

[15] a) D. H. Park, S. H. Lee, T. W. Kim, S. T. Lim, S. J. Hwang, Y. S. Yoon, Y. H. Lee, J. H. Choy, *Adv. Funct. Mater.* **2007**, *17*, 2949; b) F. Xu, Y. Xie, X. Zhang, S. Y. Zhang, X. M. Liu, W. Xi, X. B. Tian, *Adv. Funct. Mater.* **2004**, *14*, 464;

[16] a) F. Gillot, L. Monconduit, M. L. Doublet, *Chem. Mater.* **2005**, *17*, 5817; b) D. C. C. Silva, O. Crosnier, G. Ouvrard, J. Greedan, A. Safa-Sefat, L. F. Nazar, *Electrochem. Solid-State Lett.* **2003**, *8*, A162.

[17] a) L. J. Fu, H. Liu, H. P. Zhang, C. Li, T. Zhang, Y. P. Wu, R. Holze, H. Q. Wu, *Electrochem. Commun.* **2006**, *8*, 1; b) K. T. Lee, Y. S. Jung, S. M. Oh, *J. Am. Chem. Soc.* **2003**, *125*, 5652; c) J. Fan, T. Wang, C. Z. Yu, B. Tu, Z. Y. Jiang, D. Y. Zhao, *Adv. Mater.* **2004**, *16*, 1432.

[18] Y. Wang, F. B. Su, J. Y. Lee, X. S. Zhao, *Chem. Mater.* **2006**, *18*, 1347.

[19] R. K. Chiang, R. T. Chiang, *Inorg. Chem.* **2007**, *46*, 369.

[20] R. Franke, *Spectrochim. Acta, Part A* **1997**, *53*, 933.

[21] a) N. Singh, P. K. Khanna, P. A. Joy, *J. Nanoparticle Res.* **2009**, *11*, 491; b) P. K. Khanna, K.-W. Jun, K. B. Hong, J.-O. Baeg, G. K. Mehrotra, *Mater. Chem. Phys.* **2005**, *92*, 54.

[22] J. Park, E. Kang, S. U. Son, H. M. Park, M. K. Lee, J. Kim, K. W. Kim, H. J. Noh, J. H. Park, C. J. Bae, J. G. Park, T. Hyeon, *Adv. Mater.* **2005**, *17*, 429.

[23] J. L. Wang, Q. Yang, Z. D. Zhang, S. H. Sun, *Chem. Eur. J.* **2010**, *16*, 7916.

[24] A. Debart, L. Dupont, P. Poizot, J. B. Leriche, J. M. Tarascon, *J. Electrochem. Soc.* **2001**, *148*, A1266.

[25] J. B. Goodenough, Y. Kim, *Chem. Mater.* **2010**, *22*, 587.

[26] S. Grugeon, S. Laruelle, R. Herrera-Urbina, L. Dupont, P. Poizot, J. M. Tarascon, *J. Electrochem. Soc.* **2001**, *148*, A285.

[27] N. A. Kaskhedikar, J. Maier, *Adv. Mater.* **2009**, *21*, 2664.

[28] X. H. Huang, J. P. Tu, C. Q. Zhang, J. Y. Xiang, *Electrochem. Commun.* **2007**, *9*, 1180.

[29] Y. L. Ding, J. Xie, G. S. Cao, T. J. Zhu, H. M. Yu, X. B. Zhao, *Adv. Funct. Mater.* **2011**, *21*, 348.

[30] a) C. Montella, *J. Electroanal. Chem.* **2002**, *518*, 61; b) B. Dunn, J. Wang, J. Polleux, J. Lim, *J. Phys. Chem. C* **2007**, *111*, 14925.

[31] Y. Z. Chen, H. D. She, X. H. Luo, G. H. Yue, D. L. Peng, *J. Cryst. Growth* **2009**, *311*, 1229.

[32] a) H.-R. Wenk, L. Cont, Y. Xie, L. Lutterotti, L. Ratschbacher, J. Richardson, *J. Appl. Crystallogr.* **2001**, *34*, 442; b) J.-T. Han, Y.-H. Huang, W. Huang, J. B. Goodenough, *J. Am. Chem. Soc.* **2006**, *128*, 14454.